

# Modeling sparse connectivity between underlying brain sources for EEG/MEG

Stefan Haufe,<sup>\*</sup> Ryota Tomioka,<sup>†</sup> Guido Nolte,<sup>‡</sup>  
Klaus-Robert Müller and Motoaki Kawanabe

October 6, 2010

## Abstract

We propose a novel technique to assess functional brain connectivity in electro-/magnetoencephalographic (EEG/MEG) signals. Our method, called Sparsely-Connected Sources Analysis (SCSA), can overcome the problem of volume conduction by modeling neural data innovatively with the following ingredients: (a) the EEG/MEG is assumed to be a linear mixture of correlated sources following a multivariate autoregressive (MVAR) model, (b) the demixing is estimated jointly with the source MVAR parameters, (c) overfitting is avoided by using the Group Lasso penalty. This approach allows us to extract the appropriate level of cross-talk between the extracted sources and in this manner we obtain a sparse data-driven model of functional connectivity. We demonstrate the usefulness of SCSA with simulated data, and compare it to a number of existing algorithms with excellent results.

## 1 Introduction

### 1.1 Functional brain connectivity

The analysis of neural connectivity plays a crucial role for understanding the general functioning of the brain. In the past two decades such analysis has become possible thanks to tremendous progress that has been made in the fields of neuroimaging and mathematical modeling. Today, a multiplicity of imaging modalities exists, allowing us to monitor brain dynamics at different spatial and temporal scales.

Given multiple simultaneously-recorded time-series reflecting neural activity in different brain regions, a functional (task-related) connection (sometimes also called information flow or causal interaction in this paper) between two

---

<sup>\*</sup>S. Haufe and K.-R. Müller are with Berlin Institute of Technology.

<sup>†</sup>R. Tomioka is with the University of Tokyo.

<sup>‡</sup>G. Nolte and M. Kawanabe are with Fraunhofer Institute FIRST, Berlin.

regions is commonly inferred if a significant time-lagged influence between the corresponding time-series is found. Different measures have been proposed for quantifying this influence, most of them being formulated either in terms of the cross-spectrum (e.g., coherence, phase slope index [1]) or autoregressive models (e.g., Granger causality [2], directed transfer function [3], partial directed coherence [4], [5]).

## 1.2 Volume conduction problem in EEG and MEG

In electro- and magnetoencephalography (EEG and MEG), sensors are placed outside the head and the problem of volume conduction arises. That is, rather than measuring activity of only one brain site, each sensor captures a linear superposition of signals from all over the brain. This mixing introduces instantaneous correlations in the sensor data, which can cause traditional analyses to detect spurious connectivity [6].

## 1.3 Existing source connectivity analyses

Only recently methods have been brought up which qualify for EEG/MEG connectivity analysis, since they account for volume conduction effects. These methods can roughly be divided as follows.

One type of method aims at providing meaningful connectivity estimates between sensors. The idea here is that only the real part of the cross-spectrum and related quantities is affected by instantaneous effects. Thus, by using only the imaginary part, many traditional coupling measures can be made robust against volume-conduction [1, 6].

Another group of methods attempts to invert the mixing process in order to apply standard measures to the obtained source estimates. These methods can be further divided into (i) source-localization approaches (where sources are obtained as solutions to the EEG/MEG inverse problem), (ii) methods using statistical assumptions, and (iii) combined methods. The first approach is pursued, for example, in [7, 8]. Methods in the second category can be appealing, since they avoid finding an explicit inversion of the physical forward model. Instead, both the sources and the (de-)mixing transformation are estimated. To make such decomposition unique, assumptions have to be formulated, the choice of which is not so straightforward. We will now briefly review some possibilities for such assumptions.

Principal component analysis (PCA) and independent component analysis (ICA) are the most prominent linear decomposition techniques for multivariate data. Unfortunately, these methods contradict either with the goal of EEG/MEG connectivity analysis (assumption of independent sources in ICA) or even with the physics underlying EEG/MEG generation (assumption of orthogonal loadings in PCA). Nevertheless, both concepts have been used in more sophisticated ways to find EEG/MEG decompositions that better reflect physiology [9–12].

In this work, we first propose a single-step procedure to estimate all parameters (i.e. the mixing matrix and MVAR coefficients) of the linear mixing model of MVAR sources [12] based on temporal-domain convolutive ICA (CICA), instead of the combination of MVAR parameter fitting and demixing by instantaneous ICA. Furthermore, the approach enables us to integrate a sparsity assumption on brain connectivity, i.e. on interactions between *underlying brain sources*. The additional sparsity prior can avoid overfitting in practical applications and yields more interpretable estimators of brain connectivity. We remark that it is hard to incorporate such sparsity priors in MVARICA, since MVAR is fit to the (principal components of the) *sensor signals* where interactions (i.e. MVAR coefficients) are not at all sparse due to the volume conduction [12].

The remainder of the paper is organized as follows. In Section 2, our procedure will be explained step by step. The correlated source model assumed in this paper will be defined in 2.2. The identification procedure called connected sources analysis (CSA) based on the convolutive ICA will be introduced (2.3) and followed by its sparse version, sparse connected sources analysis (SCSA) with the Group Lasso prior (2.4). The relations of our methods with existing approaches such as MVARICA (i.e., MVAR+ICA, [12]) and CICAAR (convolutive ICA with an auto-regressive inverse model [13]) will be elucidated in detail (2.5). Finally, the optimization algorithms for CSA and SCSA will be explained (2.6). We implemented two versions for SCSA, one based on limited-memory Broyden–Fletcher–Goldfarb–Shanno (L-BFGS) algorithm and the other by an expectation maximization (EM) algorithm which is slower, but numerically more stable. The next section 3 will provide our experimental results on simulated data sequences emulating realistic EEG recordings. The plausibility of our correlated source model will be discussed with future research directions in the context of computational neuroscience (Section 4), before the concluding remarks (Section 5).

## 2 Connected Sources Analysis with Sparsity Prior

### 2.1 MVAR for modeling causal interactions

Autoregressive (AR) models are frequently used to define directed “Granger-causal” relations between time-series. The original procedure by Granger involves the comparison of two models for predicting a time series  $z_i$ , containing either past values of  $z_i$  and  $z_j$ , or  $z_i$  only [2]. If involvement of  $z_j$  leads to a lower prediction error, (Granger-causal) information flow from  $z_j$  to  $z_i$  is inferred. Since this may lead to spurious detection of causality if both  $z_i$  and  $z_j$  are driven by a common confounder  $z_*$ , it is advisable to include the set  $\{z_1, \dots, z_M\} \setminus \{z_i, z_j\}$  of all other observable time series in both models.

It has been pointed out, that pairwise analysis can be replaced by fitting one multivariate autoregressive (MVAR) model to the whole dataset, and that Granger-causal inference can be performed based on the estimated MVAR model coefficients (e.g., [5, 14]). Several connectivity measures are derived from the

MVAR coefficients [3, 4], but probably the following definition is most straightforward from Granger’s argument that the cause should always precede the effect. We say that time series  $z_i$  has a causal influence on time series  $z_j$  if the present and past of the combined time series  $z_i$  and  $z_j$  can better predict the future of  $z_j$  than the present and past of  $z_j$  alone. In the bivariate case this is equivalent to saying that for at least one  $p \in \{1, \dots, P\}$ , the coefficient  $H_{ji}^{(p)}$  corresponding to the interaction between  $z_j$  and  $z_i$  at the  $p$ -th time-lag is nonzero (significantly different from zero). In the multivariate case, Granger causality also includes indirect causes not contained in non-vanishing  $H_{ji}^{(p)}$ .

## 2.2 Correlated sources model

In this paper we propose a method for demixing the EEG/MEG signal into causally interacting sources. We start from the same model as in [12]: the sensor measurement is assumed to be generated as a linear instantaneous mixture of sources, which follow an MVAR model

$$\mathbf{x}(t) = M\mathbf{s}(t) \quad (1)$$

$$\mathbf{s}(t) = \sum_{p=1}^P H^{(p)}\mathbf{s}(t-p) + \boldsymbol{\varepsilon}(t). \quad (2)$$

Here,  $\mathbf{x}(t)$  is the  $D$ -dimensional EEG/MEG signal at time  $t$ ,  $M$  is a  $D \times D$  mixing matrix representing the volume conduction effect,  $\mathbf{s}(t)$  is the demixed (source) signal. The sources at time  $t$  are modeled as a linear combination of their  $P$  past values plus an innovation term  $\boldsymbol{\varepsilon}(t)$ , according to an MVAR model with coefficient matrices  $H^{(p)}$ . In the standard MVAR analysis, the innovation  $\boldsymbol{\varepsilon}(t)$  is a temporally- and spatially-uncorrelated sequence of Gaussian-distributed vectors. In contrast, we assume here that it is *i.i.d.* in time and the components are subject to non-Gaussian distributions in order to apply blind source separation (BSS) techniques based on higher-order statistics [12, 13].

For simplicity, we deal with the case that the numbers of sensors and sources are equal and the mixing matrix  $M$  is invertible. When there exist less sources than sensors, the problem falls into the current setting after being preprocessed by PCA [12]. Under our model assumptions, the innovation sequence can be obtained by a finite impulse response (FIR) filtering of the observation, i.e.

$$\boldsymbol{\varepsilon}(t) = M^{-1}\mathbf{x}(t) - \sum_{p=1}^P H^{(p)}M^{-1}\mathbf{x}(t-p) \quad (3)$$

$$= \sum_{p=0}^P W^{(p)}\mathbf{x}(t-p), \quad (4)$$

where the filter coefficients are determined by the mixing matrix  $M$  and the MVAR parameters  $\{H^{(p)}\}$  as

$$W^{(p)} = \begin{cases} M^{-1} & p = 0 \\ -H^{(p)}M^{-1} & p > 0 \end{cases}. \quad (5)$$

Eq. (3) shows a striking similarity to the convolutive ICA model [13, 15–17], where only measurements and underlying convolutive sources (here called innovations) are interchanged. Interestingly, in a somehow reverse approach, the Granger-causal interpretation of such a convolutive model was recently also discovered by [18]. Thanks to the non-Gaussianity assumption on the innovation  $\varepsilon(t)$ , we can use BSS techniques based on higher-order statistics to identify the inverse filter  $\{W^{(p)}\}$ . Since we would like to impose sparse connectivity as a plausible prior information later on, it is preferable to apply temporal-domain convolutive ICA algorithms. The obtained FIR coefficients  $\{W^{(p)}\}$  directly identify the mixing matrix  $M$  and the MVAR model of the same order  $P$ .

### 2.3 Identification by convolutive ICA

We use temporal-domain convolutive ICA for inferring volume conduction effects and causal interactions between extracted brain signals. The model parameters can be identified based on the mild assumptions that the innovations are non-Gaussian and (spatially and temporally) independent. For EEG and MEG data, a super-Gaussian is preferred to a sub-Gaussian distribution, assuming that ongoing activity of brain networks is triggered by spontaneous local bursts. We here adopt the super-Gaussian sech-distribution that was proposed in [13]. The Likelihood of the data under the model is then

$$\begin{aligned} p(\{\mathbf{x}(t)\}_{t=P+1}^T | \{W^{(p)}\}) \\ = |W^{(0)}|^{T-P} \prod_{t=P+1}^T \prod_{d=1}^D \frac{1}{\pi} \operatorname{sech}(\varepsilon_d(t)) , \end{aligned} \quad (6)$$

where  $\varepsilon(t) = M^{-1}\mathbf{x}(t) - \sum_{p=1}^P H^{(p)}M^{-1}\mathbf{x}(t-p)$  and  $T$  is the number of available time samples. The cost function to be minimized is the negative log-Likelihood

$$\begin{aligned} \mathcal{L}(\{W^{(p)}\}) &= (P-T) \log |W^{(0)}| \\ &\quad - \sum_{t=P+1}^T \sum_{d=1}^D \log \left( \frac{1}{\pi} \operatorname{sech}(\varepsilon_d(t)) \right) . \end{aligned} \quad (7)$$

The solution of Eq. (7) leads to the estimators of the mixing matrix  $M$  and the MVAR coefficients  $\{H^{(p)}\}$  via Eq. (5). We will call this procedure Connected Sources Analysis (CSA).

We remark that the temporal-domain algorithm of convolutive ICA has obvious indeterminacy due to permutations and sign flips. However, once we fix a rule to choose one from all candidates, the cost function can be considered as convex.

### 2.4 Sparse connectivity as regularization

In practice, we usually have to consider a long-range lag  $P$  to explain temporal structures of data sequences. However, this causes too many parameters to be

estimated reliably. Maximum-Likelihood estimation may easily lead to overfitting, especially if the number of observations  $T$  is small. For this reason, it is advisable to adopt a regularization scheme. Several authors have suggested that the complexity of MVAR models can be reduced by shrinking MVAR coefficients towards zero. In [14] and [19], MVAR-based functional brain connectivity is estimated from functional magnetic resonance imaging (fMRI) recordings using an  $\ell_1$ -norm based (Lasso) penalty, which has the property of shrinking some coefficients exactly to zero. In [5] it is pointed out, that, by using a so-called Group Lasso penalty [20], whole connections between time-series can be pruned at once. In this approach, all coefficients  $H_{ij}^{(p)}$ ,  $p = 1, \dots, P$  modeling the information flow from  $\mathbf{s}_i$  to  $\mathbf{s}_j$  are grouped together and can only be pruned jointly. Note that, besides MVAR modeling, such groupwise sparsification has been applied in a number of different learning tasks in neuroimaging, e.g., [21–25].

From the practical standpoint the assumption of sparse connectivity is very appealing, since fewer connections are much easier to interpret. But assuming sparse connectivity in fMRI data is also justified by studies of the numerical characteristics of network connectivity in anatomical brain databases (see [14] and the references therein). This reasoning also applies to EEG and MEG data.

We note that, besides the penalty-based approach, other strategies for obtaining sparse connectivity graphs exist. For example, post-hoc sparsification can be achieved for dense estimators by means of statistical testing [5, 26]. However, due to the compelling built-in regularization, we here adopt Group Lasso sparsification.

The sparsity assumption is only reasonable for the MVAR coefficients  $\{H^{(p)}\}$ , but not for the  $W^{(p)}$  matrices which combine MVAR coefficients and the instantaneous demixing. Hence, in order to apply sparsifying regularization, one has to split the parameters into demixing and MVAR parts again, as in the original model Eqs. (1) and (2). Since the offdiagonal elements  $\{H^{(p)}\}$  correspond to interaction between sources, we propose to put a Group Lasso penalty on them analogously to [5]. I.e., we penalize the sum of the  $\ell_2$ -norms of each of the groups  $\{H_{df}^{(p)}\}$ ,  $d \neq f$ .

Let  $B := M^{-1}(= W^{(0)})$ ,  $\mathbf{s}(t) = B\mathbf{x}(t)$  and  $\tilde{\mathbf{s}}(t) = \sum_{p=1}^P H^{(p)}\mathbf{s}(t-p)$ . The regularized cost function is

$$\begin{aligned} \mathcal{L}^{\text{SCSA}}(B, \{H^{(p)}\}) &= (P - T) \log |B| + \lambda \sum_{d \neq f} \left\| \left( H_{df}^{(1)}, \dots, H_{df}^{(P)} \right)^\top \right\|_2 \\ &\quad - \sum_{t=P+1}^T \sum_{d=1}^D \log \left( \frac{1}{\pi} \operatorname{sech}(s_d(t) - \tilde{s}_d(t)) \right), \end{aligned} \quad (8)$$

$\lambda$  being a positive constant. The solution to Eq. (8) for a choice of  $\lambda$  is called the Sparsely-Connected Sources Analysis (SCSA) estimate.

Diagonal parts of the MVAR matrices  $\{H^{(p)}\}$  model the sources' autocorrelation and should preferably not be pruned. However, in some cases numerical

stability can be increased if these variables are also penalized, especially if  $D$  and  $P$  are large. For this reason, we use a slight variation of the cost function Eq. (8) in practice, which includes

$$\lambda \left\| \left( H_{11}^{(1)}, \dots, H_{11}^{(P)}, \dots, H_{DD}^{(1)}, \dots, H_{DD}^{(P)} \right)^\top \right\|_2 \quad (9)$$

as an additional penalty term.

## 2.5 Relation to other methods

The proposed method extends previously suggested MVAR-based sparse causal discovery approaches [5, 14] by a linear demixing, which is appropriate for EEG/MEG connectivity analysis. Although the correlated sources model Eq. (1) leads to an MVAR model of the observation sequence [12], sparsity of the coefficients cannot be expected after mixing by volume conduction effects. Our method compares with MVARICA [12], which uses the same model Eq. (1), but estimates its parameters differently. More precisely, the authors of MVARICA suggest to initially fit an MVAR model in sensor-space. The demixing can then be obtained by performing instantaneous ICA on the MVAR innovations, i.e., a dedicated contrast function (Infomax) is used to model independence of the innovations. The obtained sources follow an MVAR model with time-lagged effects (interactions), but ideally no instantaneous correlations (as caused by volume conduction).

As mentioned our model Eq. (1) is very similar to the convolutive ICA model. The only difference is that Eq. (1) employs a FIR filter to extract the innovations, while an infinite response filter (IIR) is usually used in the CICA literature (see, e.g., [13]). This discrepancy is explained by the different philosophies that are associated with both methods. While in our approach the innovations  $\varepsilon(t)$  arise as residuals of a finite-length source-MVAR model, CICA understands them as sources of a finite-length convolutional (forward) mixture. Nevertheless, our unregularized cost function can be regarded as a maximum-Likelihood approach to an IIR version of convolutive ICA. This leads us also to a new view of convolutive ICA as performing an instantaneous demixing into correlated sources. Hence, it is possible to conduct source connectivity analysis using CICA (see Fig. 1 for illustration).

Compared to MVARICA and time-domain implementations of convolutive ICA such as CICAAR [13], our formulation has the advantage that sparse connectivity can easily be modeled by an additional penalty. This is not possible for CICAAR, because CICAAR only indirectly estimates the MVAR coefficients through their inverse filters. However, these are generally nonsparse, even if the true connectivity structure is sparse. Inverting the inverse coefficients is also generally not possible (recall, that convolutive ICA is equivalent to an infinite-length source-MVAR model). It is furthermore not possible to introduce a sparse regularization for MVARICA, since this method carries out the MVAR-estimation step in sensor-space, where no sparsity can be assumed.

By variation of the regularization parameter, our method is able to cover all possibilities between the extremes of a fully-correlated source model (similar to convolutive ICA) and a model which allows no cross-talk between sources. Interestingly, the latter extreme can be seen as a variant of traditional instantaneous ICA, in which independence is measured in terms of mutual predictability with a Granger-type criterion.

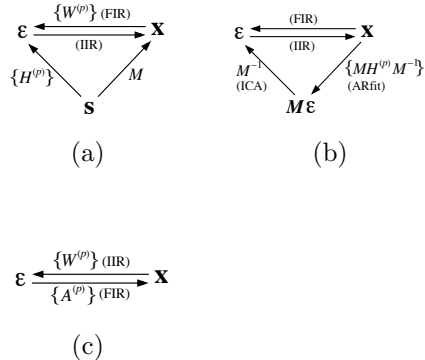


Figure 1: Relations between (a) SCSA, (b) MVARICA and (c) CICAAR. All approaches assume a non-Gaussian innovation sequence  $\varepsilon$ . SCSA and MVARICA fit an IIR model to the observed sequence  $\mathbf{x}$ , while CICAAR assumes an FIR filter for it. Therefore, in SCSA and MVARICA the inverse filter from  $\mathbf{x}$  to the innovation  $\varepsilon$  is an FIR. MVARICA is a two step approach with AR fitting to the observed sequence  $\mathbf{x}$  and spartial demixing of the innovation  $M\varepsilon$  obtained in the first step. On the other hand, SCSA is a one-step approach which compute the inverse FIR filter by convolutive ICA. We remark that the AR fitting in MVARICA relies only on the second order statistics, which may cause the performance drops compared to CSA.

## 2.6 Optimization

### 2.6.1 CSA

The gradient of the unregularized cost function Eq. (7) is obtained as

$$\begin{aligned} \frac{\partial \mathcal{L}}{\partial W_d^{(p)}} &= \delta(p) \left( (P - T) W^{(p)-\top} \mathbf{e}_d \right) \\ &+ \sum_{t=P+1}^T \tanh \left( \sum_{p=0}^P W_d^{(p)\top} \mathbf{x}(t-p) \right) \mathbf{x}(t-p), \end{aligned} \quad (10)$$

where  $W_d^{(p)} := W^{(p)\top} \mathbf{e}_d$ , i.e. the  $d$ -th column vector of  $W^{(p)\top}$ . Using Eq. (10), CSA can be readily solved by means of an L-BFGS optimizer [27]<sup>1</sup>.

<sup>1</sup>We use an implementation by Naoaki Okazaki, <http://www.chokkan.org/software/liblbfgs/>.



### 2.6.2 SCSA via a modified L-BFGS algorithm

Using sparse regularization, two difficulties emerge compared to the unregularized cost function. First, using the factorization Eq. (5), the cost function is likely to have local minima, which might be found instead of the true global minimum. Furthermore, the function Eq. (8) is not differentiable, when one of the terms  $\|(H_{df}^{(1)}, \dots, H_{df}^{(P)})^\top\|_2, d \neq f$  becomes zero, which is expected to be the case at the optimum. For tackling these difficulties we here propose to use a modified version of the L-BFGS algorithm, which allows joint nonlinear optimization of  $B$  and  $\{H^{(p)}\}$ , while taking special care of the nondifferentiability of the regularizer. The gradient of Eq. (8) for the case  $d \neq f$  is obtained as

$$\begin{aligned} \frac{\partial \mathcal{L}^{\text{SCSA}}}{\partial H_{df}^{(p)}} &= - \sum_{t=P+1}^T \tanh(s_d(t) - \tilde{s}_d(t)) s_f(t-p) \\ &\quad + \lambda \frac{H_{df}^{(p)}}{\left\| \left( H_{df}^{(1)}, \dots, H_{df}^{(P)} \right)^\top \right\|_2} \end{aligned} \quad (11)$$

(analogously for  $d \equiv f$ ) and

$$\begin{aligned} \frac{\partial \mathcal{L}^{\text{SCSA}}}{\partial B_d} &= (P-T)B^{-\top} \mathbf{e}_d \\ &\quad + \sum_{t=P+1}^T \sum_{d=1}^D \left\{ \tanh(s_d(t) - \tilde{s}_d(t)) \right. \\ &\quad \left. \times \left( \mathbf{x}(t) - \sum_{p=1}^P x_d(t-p) H_d^{(p)} \right) \right\} . \end{aligned} \quad (12)$$

Our modified L-BFGS algorithm checks before each gradient evaluation, whether  $\|(H_{11}^{(1)}, \dots, H_{11}^{(P)}, \dots, H_{DD}^{(1)}, \dots, H_{DD}^{(P)})^\top\|_2$  or some of the terms  $\|(H_{df}^{(1)}, \dots, H_{df}^{(P)})^\top\|_2, d \neq f$  are already (close to) zero. If any of the terms equals zero, the gradient is not defined uniquely but as a set (subdifferential). Nevertheless it is straightforward to compute the element of the subdifferential with the minimum norm, whose sign inversion is always a descent direction. Care must be taken because in practice we would not find any of the above terms exactly equal to zero. Thus we truncate the elements of  $H$  corresponding to the terms with small norms below some threshold to zero before computing the minimum norm subgradient. If the minimum is indeed attained at the truncated point, the minimum norm subgradient will be zero. Otherwise the subgradient will drive the solution out of zero. Further care must be taken in practice to prevent the solution from oscillating in and out of some zero.

We find that, using the outlined optimization procedure, sparse solutions can be found in shorter time, if the solution of the unregularized cost function

is used as the initializer. The starting point can be obtained using the inverse transformation of Eq. (5).

### 2.6.3 SCSA via an EM algorithm

Using joint optimization of  $B$  and  $\{H^{(p)}\}$ , the heuristic pruning of connections might in some cases lead to suboptimal solutions regarding the composite cost function. For this reason, we present an alternative optimization scheme, which does not require any heuristic step. The idea here is to alternate between the estimation of both unknowns. Doing so can be justified as an application of the EM algorithm (see [28]).

Estimation of  $B$  given  $\{H^{(p)}\}$  (here called E-step) amounts to solving an unconstrained nonlinear optimization problem. Importantly this problem is also convex, in contrast to the joint approach to SCSA parameter fitting. The convexity follows from the concavity of  $\log |X|$  and  $\log(\text{sech}(ax))$  for constant  $a$  (and from the fact that the sum of convex functions is convex.). The great advantage of convex problems is, that they feature a unique (local and global) minimum. In our case, the objective is smooth, so the minimum is guaranteed to be found by the L-BFGS algorithm, making use of the gradient in Eq. (12).

Optimization with respect to  $\{H^{(p)}\}$  for fixed  $B$  (M-step) is more involved, since the nondifferentiable Group Lasso regularizer remains. Smooth optimization methods like L-BFGS are unlikely to find the exact solution here. However, this problem is not as difficult as the joint optimization problem, since it is convex. This can be seen from the fact that it is composed of a sum of  $-\log(\text{sech}(ax))$  terms (loss function) and the Group Lasso term (regularizer), which is a sum of  $\ell_2$ -norms and thus convex. Hence we can solve this problem using the Dual Augmented Lagrangian (DAL) procedure [29], which has recently been introduced as a method for minimizing arbitrary convex loss functions with additional Lasso or Group Lasso penalties. Application of DAL requires the loss function and its gradient, the convex conjugate (Legendre transform) of the loss function, as well as gradient and Hessian of the conjugate loss. Let  $\mathbf{s}(t) = B\mathbf{x}(t)$  be the demixed sources and  $\tilde{\mathbf{s}}(t) = \sum_{p=1}^P H^{(p)}\mathbf{s}(t-p)$  be their autoregressive approximations. The loss function in terms of  $\tilde{\mathbf{s}}$  is defined as

$$\mathcal{L}^M(\tilde{\mathbf{s}}) = - \sum_{t=P+1}^T \sum_{d=1}^D \log \left( \frac{1}{\pi} \text{sech}(\tilde{s}_d(t) - s_d(t)) \right). \quad (13)$$

The gradient is

$$\frac{\partial \mathcal{L}^M}{\partial \tilde{s}_d(t)} = \tanh(\tilde{s}_d(t) - s_d(t)). \quad (14)$$

Let  $\mathbf{a}_d(t)$  ( $d = 1, \dots, D, t = P+1, \dots, T$ ) denote the dual variables associated with the Legendre transform. The conjugate loss function is defined on the

interval  $[-1, 1]$  and evaluates to

$$\begin{aligned}
\mathcal{D}^M(\mathbf{a}) &= \sum_{t=P+1}^T \sum_{d=1}^D \sup_{\tilde{s}_d(t)} \left( -\mathbf{a}_d(t)\tilde{s}_d(t) + \log \frac{\operatorname{sech}(\tilde{s}_d(t) - s_d(t))}{\pi} \right) \\
&= \sum_{t=P+1}^T \sum_{d=1}^D \left( \frac{1 - \mathbf{a}_d(t)}{2} \log \frac{1 - \mathbf{a}_d(t)}{2} \right. \\
&\quad \left. + \frac{1 + \mathbf{a}_d(t)}{2} \log \frac{1 + \mathbf{a}_d(t)}{2} - \mathbf{a}_d(t)s_d(t) + \log \frac{2}{\pi} \right). \tag{15}
\end{aligned}$$

The gradient of the conjugate loss is given by

$$\frac{\partial \mathcal{D}^M(\mathbf{a})}{\partial \mathbf{a}_d(t)} = \frac{1}{2} \log \frac{1 + \mathbf{a}_d(t)}{1 - \mathbf{a}_d(t)} - s_d(t). \tag{16}$$

The Hessian is diagonal with elements

$$\frac{\partial^2 \mathcal{D}^M(\mathbf{a})}{\partial \mathbf{a}_d(t)^2} = \frac{1}{2(1 - \mathbf{a}_d^2(t))}. \tag{17}$$

Having defined the E- and M-steps, we have turned a nonconvex estimation problem into a sequence of two convex problems, which can both be solved exactly. A final estimate of the model parameters can now be obtained by alternating between E- and M-steps until convergence.

### 3 Performance under realistic conditions

We conducted the following simulations in order to assess the performance of the proposed source connectivity analysis compared to those of existing approaches.

#### 3.1 Data generation

We simulated seven time-series (pseudo-sources) of length  $N = 2000$  according to an MVAR model of order  $P = 4$ . Seven out of the forty-two possible interactions were modeled by allowing the corresponding offdiagonal MVAR coefficients  $H_{df}^{(p)}$ ,  $d \neq f$ ,  $1 \leq p \leq P$  to be nonzero. The innovations were drawn from the sech-distribution (Note that the assumption of non-Gaussianity is crucial for recovering mixed sources.).

The pseudo-sources were mapped to 118 EEG channels using the theoretical spread of seven randomly placed dipoles. The spread was computed using a realistic forward model [30] which was built based on anatomical MR images of the ‘‘Montreal head’’ [31]. See Fig. 2 for an example illustrating the data generation.

In reality, measurements are never noise-free and the following model holds rather than Eq. (1)

$$\mathbf{x}(t) = M\mathbf{s}(t) + \boldsymbol{\xi}(t). \quad (18)$$

Since none of the methods compared here (see below) explicitly models a noise term, it is important to evaluate their robustness to model violation. To this end, we constructed additional variants of the pseudo-EEG dataset by adding six different types of noise  $\boldsymbol{\xi}$ . The six variants (N1-N6) are summarized in TABLE 1. These variants differ in their degree of spatial and temporal correlation as follows. In variants N1 and N4,  $\xi_i(t), i = 1, \dots, M$  were drawn independently for each sensor, i.e., have no spatial correlation. For variants N2 and N5 noise terms  $\xi_i^*(t), i = 1, \dots, D$  were drawn independently for each *source*. In this case, sources and noise contributions to the EEG share the same covariance given by the mixing matrix  $M$ , i.e.,  $\mathbf{x}(t) = M(\mathbf{s}(t) + \boldsymbol{\xi}^*(t))$ . For the last variants N3 and N6, spatially independent noise sources were simulated at all nodes of a grid covering the whole brain, yielding the model  $\mathbf{x}(t) = M\mathbf{s}(t) + M^*\boldsymbol{\xi}^*(t)$ . Here, in contrast to the previous model, noise contributions are not collinear to the sources. We further distinguish between noise sources with and without temporal structure. In variants (N1-N3), noise terms were drawn *i.i.d.* (independent and identically distributed) from a normal distribution at each time instant  $t$ . In variants N4-N6, the temporal structure was determined by a *univariate* AR model of order 20, i.e.,  $\xi_i(t) = \sum_{p=1}^{20} h^{(p)}\xi_i(t-p) + \varepsilon(t)$  for noise type N4.

Note that, since no time-delayed dependencies between noise sources were modeled, no additional Granger-causal effects were introduced by the noise. We used a signal-to-noise ratio (SNR) of 2 in all experiments, where SNR is defined as

$$\text{SNR} = \frac{\|M(\mathbf{s}(1), \dots, \mathbf{s}(T))\|_{\mathcal{F}}}{\|\boldsymbol{\xi}(1), \dots, \boldsymbol{\xi}(T)\|_{\mathcal{F}}}, \quad (19)$$

and  $\|\cdot\|_{\mathcal{F}}$  is the Frobenius norm (sum of squared entries) of a matrix. One-hundred datasets with different realisations of MVAR coefficients, innovations and noise were constructed for each category.

We performed two additional experiments (100 repetitions each) in order to investigate the performance of the various methods under variation of the connectivity structure of the underlying sources, as well as the SNR. Seven degrees of connectedness (from 0% to 100%) and seven choices of the SNR (from 1 to 4) were considered. These ranges included the parameters used in the previous experiments (17% = 7/42 of all possible interactions present, SNR=2). SNR variation was investigated using white sensor noise without temporal structure (N1), while the effect of connectivity was studied for the noiseless case.

In all experiments, PCA-based dimensionality reduction was applied to the pseudo-EEG by taking just the strongest signal components. Since our evalu-

ation scheme relies on a one-to-one mapping between estimated and true components (see Section 3.3), we here used exactly as many dimensions as original sources  $D = 7$ . In practice, this information is of course not available and the number of dimensions can be chosen such that, for instance, 99% of the variance in the EEG is explained. Our experience here shows that taking too many dimensions is generally less harmful than the opposite, since spare dimensions can just be used to dump noise.

Table 1: The six types of noise used in the simulations. Noise with temporal correlation structure was created using univariate AR models of order 20. Spatial correlation was introduced using the forward model. We distinguish between the case, where noise sources coincide with the true dipoles <sup>(a)</sup> and the case in which noise from all brain sites contributes to the measurements <sup>(b)</sup>.

	independent in time	correlated in time
independent in sensors	N1	N4
correlated in sensors <sup>a</sup>	N2	N5
correlated in sensors <sup>b</sup>	N3	N6

### 3.2 Methods

We tested the ability of ICA, MVARICA, CICAAR and the two proposed methods CSA and SCSA to reconstruct the seven sources and their connectivity structure. Although the goal of instantaneous ICA is fundamentally different to source connectivity analysis, it was also included here in the comparison. This is since, even if independence of the sources is not fulfilled, ICA might still provide minimally dependent components, the connectivity of which might be analyzed. The ICA variant used here is based on temporal decorrelation [32–35] (implemented by fast approximate joint diagonalization [36]). The number of temporal lags was set to 100.

MVARICA, CICAAR, CSA and SCSA were tested with  $P \in \{1, 2, \dots, 7\}$  temporal lags, where four is the true MVAR model order for CSA, SCSA and MVARICA. CICAAR has the disadvantage here, that it may generally require extended temporal filters for reconstructing sources following model Eq. (1). However, due to computation time constraints,  $P = 7$  was taken as the maximum lag also for this method. For MVARICA and CICAAR, we used implementations provided by the respective authors. These implementations adopt the Bayesian Information Criterion (BIC) for selecting the appropriate number of time lags. The same criterion was used to select the model order in CSA and SCSA. The regularization constant  $\lambda$  of SCSA was set by 5-fold cross-validation, i.e. by evaluating the likelihood on test data. SCSA estimates of  $\{H^{(p)}\}$  and  $B$  were obtained either jointly using the modified L-BFGS algorithm or alternately

using 20 additional EM steps. These variants are named SCSA and SCSA\_EM here, respectively.

### 3.3 Performance measures

The most important performance criterion is the reconstruction of the mixing matrix, since all other relevant quantities can basically be derived from it. All considered methods provide an estimate  $\hat{M}^{-1}$  of the demixing, which can be inverted to yield an estimated mixing matrix. The columns of the mixing matrix correspond to spatial field patterns of the estimated sources, but unfortunately these patterns can generally only be determined up to sign, scale and order. For this reason, optimal pairing of true and estimated patterns as described in [37] was performed. Compared to we used a slightly modified similarity measure, which was the goodness-of-fit achieved by a linear least-squares regression of one to another pattern. For a true pattern  $M_d$  and an estimated pattern  $\hat{M}_f$  the optimal regression coefficient is

$$c(M_d, \hat{M}_f) = \frac{\hat{M}_f^\top M_d}{\|\hat{M}_f\|^2} \quad (20)$$

and the goodness-of-fit (GOF) is

$$\text{GOF}(M_d, \hat{M}_f) = \frac{\|c\hat{M}_f - M_d\|}{\|M_d\|}. \quad (21)$$

Having found the optimal pairing, the columns of  $M$  were permuted and scaled to approximate  $M$  as good as possible using the optimal regression coefficients. The goodness-of-fit with respect to the whole matrix  $M$  was used to evaluate the quality of the different decompositions. Additionally, using the optimally-matched mixing patterns, dipole scans were conducted. That is, for each discrete location in the brain (5mm grid size) a dipolar current source was fitted. The location of the dipole that best explains the EEG pattern was determined. The deviation of these locations from the true ones was measured. A typical example of a mixing pattern estimated by SCSA and the corresponding reconstructed dipole is shown in Fig. 2.

Finally, causal discovery according to [5] was carried out on the demixed sources. The exact technique used was MVAR estimation with Ridge Regression. For the MVAR parameters estimated by Ridge Regression an approximate multivariate Gaussian distribution can be derived, which was used to test the coefficients for being significantly different from zero. An influence from  $s_i$  to  $s_j$  was defined, if the  $p$ -value of one of the coefficients  $H_{ij}^{(p)}$ ,  $p = 1, \dots, P$  fell below the critical value. As a third performance criterion, the area under curve (AUC) score for correctly discovering the interaction structure was calculated by varying the significance threshold and comparing estimated and true connectivity matrix for each threshold. Note that this way of connectivity estimation was pursued here, since not all demixing methods provide built-in connectivity

estimates. For SCSA, however, interaction analysis could as well have been done by directly examining MVAR coefficients.

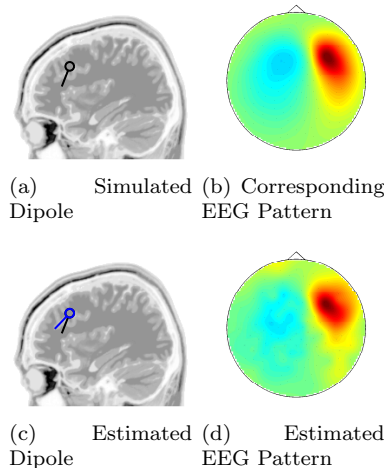


Figure 2: Example of simulated data (noise type N1) and corresponding reconstruction by SCSA. (a) Simulated dipole. (b) Field pattern describing the dipole’s influence on the EEG (one column of  $M$ ). (d) Field pattern as estimated by SCSA from noisy EEG time series. (c) Reconstructed dipole, obtained from the estimated pattern.

### 3.4 Results

Fig. 3 shows how well the mixing matrix was approximated by the different approaches. One boxplot is drawn for the noiseless case (N0) and each of the six noisy variants (N1-N6, see Table 1). The plots show the median performance over 100 repetitions, as well as the lower and upper quartiles and the extremal values. Outliers (red crosses) were removed. As a result of the simulations, SCSA typically achieves the smallest reconstruction error, followed by CSA, CICAAR, MVARICA and ICA. In many cases, the differences are also significant (non-overlapping notches of two boxes indicate that the two medians differ at the 5% significance level).

Correct (de-)mixing matrix estimation affects both the localization error achievable by applying inverse methods to the estimated patterns and the error of any connectivity analysis performed at the demixed sources. As a result of good mixing matrix approximation, SCSA also achieves smaller dipole localization errors than all other methods, except in one scenario (shown in Fig. 4). The same situation occurs when it comes to estimating the connectivity between sources (Fig. 5).

Regarding noise influence it might be said that the relative degradation of

performance in the presence of noise is the same for all methods. Generally, noise that is collinear to the sources (N2/N5) leads to higher performance than noise that is uncorrelated across sensors (N1/N4) and noise with arbitrary spatial correlation structure (N3/N6). These differences are partially explained with the effectiveness of the PCA step performed for dimensionality reduction. The average total variance explained by the PCA subspace was 96% for noise types N1/N4 and 81% for noise types N3/N6, while it was 100% for collinear noise N2/N5. As a consequence, we suggest that in practice a 99% rule should be most suitable, even if the number of sources can be roughly estimated.

As shown in the right panel of Fig. 6 the performance of all methods decays with decreasing SNR, while the difference between methods remains rather stable across SNR levels. The left panel of that Figure shows that the superiority of methods proposed here (SCSA and SCSA) over CICAAR, MVARICA and ICA is stable even under variation of the degree of connectedness. Only, SCSA variants seem to lose their advantage over CSA in cases of very dense connectivity structure. This is somewhat unexpected, since SCSA does provide a mechanism (evaluation of the out-of-sample prediction error) to adjust to the actual amount of connectivity. In some cases, the data could apparently be better explained by models with fewer source connections than actually present, which might have numerical reasons.

The time each method consumed on average for processing one dataset is shown in Fig. 7. Most methods finish in rather short time, while the EM implementation of SCSA is in medium range and CICAAR requires the longest time. However, for SCSA there is still room for improvement, since the regularization parameter of this method is currently selected by the cross-validation procedure, which could be changed.

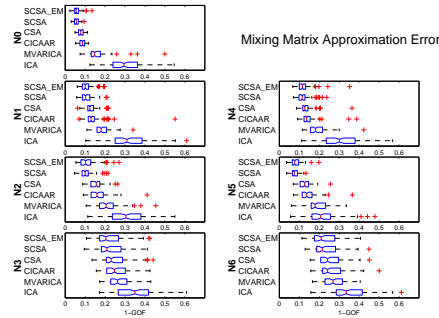


Figure 3: Estimation errors of the mixing matrix according to the goodness-of-fit (GOF) criterion. Results are shown for the proposed (Sparsely-) Connected Sources Analysis variants (SCSA\_EM, SCSA, CSA) and three alternative approaches (CICAAR, MVARICA, ICA). Different subfigures depict the methods’ performance in the noiseless case (N0), as well as in the presence of different types of noise (N1-N6, see TABLE 1).



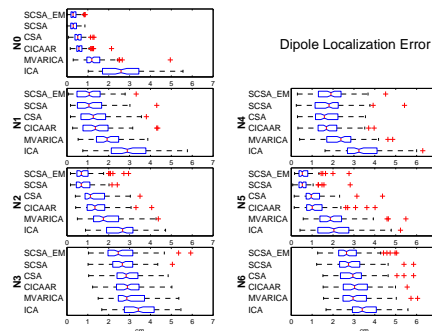


Figure 4: Localization errors of dipole fits conducted on the estimated mixing field patterns. Results are shown for the proposed (Sparsely-) Connected Sources Analysis (SCSA\_EM, SCSA, CSA) variants and three alternative approaches (CICAAR, MVARICA, ICA). Different subfigures depict the methods’ performance in the noiseless case (N0), as well as in the presence of different types of noise (N1-N6, see TABLE 1).

## 4 Discussion

Let us recall the assumptions we make to identify individual brain sources and to estimate their interactions. While ICA results in a unique decomposition assuming statistical independence, such an assumption is inconsistent when studying brain interactions. However, all neural interactions require a minimum delay well within the temporal resolution of electrophysical measurements of brain activity. Hence, it makes sense to assume independent innovation processes and to model all interactions explicitly using AR matrices. In relation to ICA we pay some price for that: In our case, independence is exploited effectively on reduced information contained in the residuals of the model. In principle, this can be a cause for less stable estimates. To increase stability, we have included sparsity assumptions based on the idea that only a few brain connections can be as strong to be observable in EEG data which is especially the case in the presence of artifacts and background noise.

We emphasize that BSS methods exploiting higher order statistics without using temporal information would fail completely if the data were Gaussian distributed (cf. the empirical evaluation by [12]). Processes tend to be super-Gaussian if they are not always active, which is a reasonable assumption for brain sources and even more so for artifacts which also need to be included in the model. Here we assume a linear dynamical model and super-Gaussian innovation processes, i.e. the only cause of non-Gaussianity is the innovation process itself. Real brain networks are, of course, more complicated. However, the question whether nonlinear dynamical models may improve the results or are even essential for a correct decomposition is beyond the scope of this paper and will be addressed in the future. Similarly, we assumed the total number of

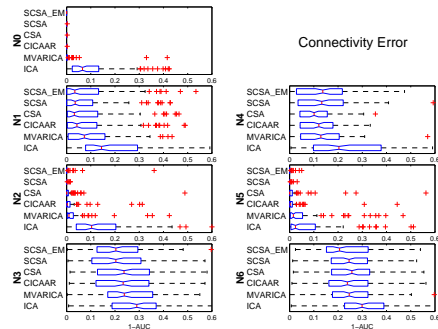


Figure 5: Estimation errors regarding the source connectivity structure as measured by fitting an MVAR model subsequently to the demixed sources and testing the obtained coefficients for significant interaction. The performance measure reported is the area under the curve (AUC) score obtained by varying the significance level.

sources to be less or equal the number of channels. Apparently, the significance of this problem decreases when using a large number of channels.

## 5 Conclusion

Analyzing functional brain connectivity is a challenging problem, since volume conduction effects in EEG/MEG measurements can give rise to spurious effects. In this work we have established a novel connectivity analysis method SCSA that overcomes these problems in an elegant and numerically appealing manner. In detail, EEG/MEG is modeled as a linear mixture of correlated sources, then we estimate jointly the demixing process and the MVAR model (which is the model basis for the correlated sources). To avoid overfitting we regularize the model using the Group Lasso penalty. In this manner we can achieve a data driven interpolation between two extremes: a source model that has full correlations and one that does not allow for cross-talk between the extracted sources. In between, our method extracts a sparse connectivity model.

Future work will study the link between methods for compensating non-stationarity in data such as Stationary Subspace Analysis (SSA, [38]) and our novel connectivity assessment. In addition, we aim to localize the extracted components of connectivity using distributed source models to enhance physiological interpretability (e.g. [22, 39]). A third field of upcoming research is the extension of our causal model to multi-way data by building on the work of [40].

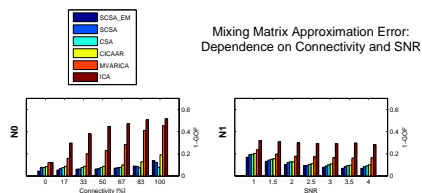


Figure 6: Mixing matrix approximation performance of (Sparsely-) Connected Sources Analysis variants (SCSA\_EM, SCSA, CSA) and three alternative approaches (CICAAR, MVARICA, ICA) under variation of the degree of connectiveness (left side) and SNR (right side). The performance at different noise levels is investigated for white sensor noise without temporal structure (N1), while the influence of connectivity is studied in the noiseless case (N0).

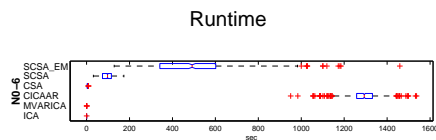


Figure 7: Average runtime of the proposed (Sparsely-) Connected Sources Analysis variants (SCSA\_EM, SCSA, CSA) and three alternative approaches (CICAAR, MVARICA, ICA), taken over all experiments conducted for this study.

## Acknowledgement

This work was partly supported by the *Bundesministerium für Bildung und Forschung* (BMBF), Fkz 01GQ0850 and by the European ICT Programme Project FP7-224631 and 216886. We thank Germán Gómez Herrero and Mads Dyrholm for making the source code of their algorithms available, and Nicole Krämer for discussions.

## References

- [1] G. Nolte, A. Ziehe, V. V. Nikulin, A. Schlögl, N. Krämer, T. Brismar, and K. R. Müller, “Robustly estimating the flow direction of information in complex physical systems,” *Phys. Rev. Lett.*, vol. 100, p. 234101, Jun 2008.
- [2] C. Granger, “Investigating causal relations by econometric models and cross-spectral methods,” *Econometrica*, vol. 37, pp. 424–438, 1969.
- [3] M. J. Kaminski and K. J. Blinowska, “A new method of the description of the information flow in the brain structures,” *Biol Cybern*, vol. 65, pp. 203–210, 1991.

- [4] L. A. Baccalá and K. Sameshima, “Partial directed coherence: a new concept in neural structure determination,” *Biol Cybern*, vol. 84, pp. 463–474, Jun 2001.
- [5] S. Haufe, G. Nolte, K.-R. Müller, and N. Krämer, “Sparse causal discovery in multivariate time series,” *JMLR W&CP*, vol. 6, pp. 97–106, 2010.
- [6] G. Nolte, O. Bai, L. Wheaton, Z. Mari, S. Vorbach, and M. Hallett, “Identifying true brain interaction from EEG data using the imaginary part of coherency,” *Clin. Neurophysiol.*, vol. 115, pp. 2292–2307, Oct 2004.
- [7] A. G. Guggisberg, S. M. Honma, A. M. Findlay, S. S. Dalal, H. E. Kirsch, M. S. Berger, and S. S. Nagarajan, “Mapping functional connectivity in patients with brain lesions,” *Ann. Neurol.*, vol. 63, pp. 193–203, Feb 2008.
- [8] L. Astolfi, F. Cincotti, D. Mattia, C. Babiloni, F. Carducci, A. Basilisco, P. M. Rossini, S. Salinari, L. Ding, Y. Ni, B. He, and F. Babiloni, “Assessing cortical functional connectivity by linear inverse estimation and directed transfer function: simulations and application to real data,” *Clin Neurophysiol*, vol. 116, pp. 920–932, Apr 2005.
- [9] L. Marzetti, C. Del Gratta, and G. Nolte, “Understanding brain connectivity from EEG data by identifying systems composed of interacting sources,” *NeuroImage*, vol. 42, pp. 87–98, Aug 2008.
- [10] G. Nolte, L. Marzetti, and P. Valdes Sosa, “Minimum Overlap Component Analysis (MOCA) of EEG/MEG data for more than two sources,” *J. Neurosci. Methods*, vol. 183, pp. 72–76, Sep 2009.
- [11] P. A. Valdés-Sosa, M. Vega-Hernández, J. M. Sánchez-Bornot, E. Martínez-Montes, and M. A. Bobes, “EEG source imaging with spatio-temporal tomographic nonnegative independent component analysis,” *Hum Brain Mapp*, vol. 30, pp. 1898–1910, Jun 2009.
- [12] G. Gómez-Herrero, M. Atienza, K. Egiazarian, and J. L. Cantero, “Measuring directional coupling between EEG sources,” *NeuroImage*, vol. 43, pp. 497–508, Nov 2008.
- [13] M. Dyrholm, S. Makeig, and L. K. Hansen, “Model selection for convolutive ICA with an application to spatiotemporal analysis of EEG,” *Neural Comput*, vol. 19, pp. 934–955, Apr 2007.
- [14] P. A. Valdés-Sosa, J. M. Sánchez-Bornot, A. Lage-Castellanos, M. Vega-Hernández, J. Bosch-Bayard, L. Melie-García, and E. Canales-Rodríguez, “Estimating brain functional connectivity with sparse multivariate autoregression,” *Philosophical Transactions of the Royal Society B*, vol. 360, pp. 969–981, 2005.

- [15] H. Attias and C. E. Schreiner, “Blind source separation and deconvolution: the dynamic component analysis algorithm,” *Neural Comput.*, vol. 10, pp. 1373–1424, Aug 1998.
- [16] L. Parra and C. Spence, “Convulsive blind source separation of non-stationary sources,” *IEEE Trans. Speech Audio Processing*, vol. 8, no. 3, pp. 320–327, 2000.
- [17] J. Anemüller, T. J. Sejnowski, and S. Makeig, “Complex independent component analysis of frequency-domain electroencephalographic data,” *Neural Netw.*, vol. 16, pp. 1311–1323, Nov 2003.
- [18] M. Mørup, K. H. Madsen, and L. K. Hansen, “Latent causal modelling of neuroimaging data,” 2009. [Online]. Available: <http://www2.imm.dtu.dk/pubdb/p.php?5804>
- [19] J. M. Sánchez-Bornot, E. Martínez-Montes, A. Lage-Castellanos, M. Vega-Hernández, and P. A. Valdés-Sosa, “Uncovering sparse brain effective connectivity: A voxel-based approach using penalized regression,” *Statistica Sinica*, vol. 18, no. 4, 2008.
- [20] M. Yuan and Y. Lin, “Model selection and estimation in regression with grouped variables,” *J. Roy. Stat. Soc. B Meth.*, vol. 68, no. 1, pp. 49–67, 2006.
- [21] S. F. Cotter, B. D. Rao, K. Engan, and K. Kreutz-Delgado, “Sparse solutions to linear inverse problems with multiple measurement vectors,” *IEEE Trans. Signal Proces.*, vol. 53, pp. 2477–2488, 2005.
- [22] S. Haufe, V. Nikulin, A. Ziehe, K.-R. Müller, and G. Nolte, “Combining sparsity and rotational invariance in EEG/MEG source reconstruction,” *NeuroImage*, vol. 42, no. 2, pp. 26–738, 2008.
- [23] M. van Gerven, C. Hesse, O. Jensen, and T. Heskes, “Interpreting single trial data using groupwise regularisation,” *NeuroImage*, vol. 46, pp. 665–676, 2009.
- [24] D. Wipf and S. Nagarajan, “A unified Bayesian framework for MEG/EEG source imaging,” *Neuroimage*, vol. 44, pp. 947–966, Feb 2009.
- [25] R. Tomioka and K. R. Muller, “A regularized discriminative framework for EEG analysis with application to brain-computer interface,” *NeuroImage*, vol. 49, pp. 415–432, Jan 2010.
- [26] D. Marinazzo, M. Pellicoro, and S. Stramaglia, “Kernel method for nonlinear Granger Causality,” *Phys. Rev. Lett.*, vol. 100, p. 144103, 2008.
- [27] J. Nocedal, “Updating quasi-newton matrices with limited storage,” *Mathematics of Computation*, vol. 35, no. 151, pp. 773–782, 1980. [Online]. Available: <http://www.jstor.org/stable/2006193>

- [28] R. Neal and G. E. Hinton, “A view of the EM algorithm that justifies incremental, sparse, and other variants,” in *Learning in Graphical Models*. Kluwer Academic Publishers, 1998, pp. 355–368.
- [29] R. Tomioka and M. Sugiyama, “Dual augmented lagrangian method for efficient sparse reconstruction,” *IEEE Signal Proc Let*, vol. 16, no. 2, pp. 1067–1070, 2009.
- [30] G. Nolte and G. Dassios, “Analytic expansion of the EEG lead field for realistic volume conductors,” *Phys. Med. Biol.*, vol. 50, pp. 3807–3823, 2005.
- [31] C. J. Holmes, R. Hoge, L. Collins, R. Woods, A. Toga, and A. C. Evans, “Enhancement of MR images using registration for signal averaging,” *J. Comput. Assist. Tomogr.*, vol. 22, no. 2, pp. 324–333, 1998.
- [32] L. Molgedey and H. G. Schuster, “Separation of a mixture of independent signals using time delayed correlations,” *Phys. Rev. Lett.*, vol. 72, pp. 3634–3637, Jun 1994.
- [33] A. Belouchrani, K. Abed-Meraim, J. F. Cardoso, and E. Moulines, “A blind source separation technique using second-order statistics,” *IEEE Trans Signal Proc*, vol. 45, no. 2, pp. 434–444, August 1997. [Online]. Available: <http://dx.doi.org/10.1109/78.554307>
- [34] A. Ziehe and K.-R. Müller, “TDSEP—an efficient algorithm for blind separation using time structure,” *Proc. Int. Conf. on Artificial Neural Networks (ICANN '98)*, pp. 675–680, 1998.
- [35] A. Ziehe, K.-R. Müller, G. Nolte, and B.-M. Mackert. and G. Curio, “Artifact reduction in magnetoneurography based on time-delayed second-order correlations,” *IEEE Trans Biomed Eng*, vol. 47, no. 1, pp. 75–87, 2000.
- [36] A. Ziehe, P. Laskov, G. Nolte, and K.-R. Müller, “A fast algorithm for joint diagonalization with non-orthogonal transformations and its application to blind source separation,” *J. Mach. Learn. Res.*, vol. 5, pp. 777–800, 2004. [Online]. Available: <http://portal.acm.org/citation.cfm?id=1016784>
- [37] P. Tichavský and Z. Koldovský, “Optimal pairing of signal components separated by blind techniques,” *IEEE Signal Proc Let*, vol. 11, no. 2, pp. 119–122, 2004.
- [38] P. von Büнау, F. C. Meinecke, F. Király, and K.-R. Müller, “Finding stationary subspaces in multivariate time series,” *Physical Review Letters*, vol. 103, p. 214101, 2009.
- [39] S. Haufe, V. V. Nikulin, A. Ziehe, K.-R. Müller, and G. Nolte, “Estimating vector fields using sparse basis field expansions,” in *Advances in Neural Information Processing Systems 21*, D. Koller, D. Schuurmans, Y. Bengio, and L. Bottou, Eds., 2009, pp. 617–624.

- [40] M. Mørup, L. K. Hansen, S. M. Arnfred, L. H. Lim, and K. H. Madsen, “Shift-invariant multilinear decomposition of neuroimaging data,” *NeuroImage*, vol. 42, pp. 1439–1450, Oct 2008.